NeuroImage 87 (2014) 395–402

Contents lists available at ScienceDirect

NeuroImage

journal homepage: www.elsevier.com/locate/ynimg

PET imaging of demyelination and remyelination in the cuprizone mouse model for multiple sclerosis: A comparison between [^{11}C]CIC and [^{11}C]MeDAS

Daniele de Paula Faria [a,b,c], Erik F.J. de Vries [a,*], Jurgen W.A. Sijbesma [a], Rudi A.J.O. Dierckx [a], Carlos A. Buchpiguel [c], Sjef Copray [b]

[a] Department of Nuclear Medicine and Molecular Imaging, University of Groningen, University Medical Center Groningen, Groningen 9713 GZ, The Netherlands
[b] Department of Neuroscience, University of Groningen, University Medical Center Groningen, Groningen 9713 GZ, The Netherlands
[c] Center of Nuclear Medicine, University of Sao Paulo, University of Sao Paulo Medical School, Sao Paulo 05403-900, Brazil

ARTICLE INFO

Article history:
Accepted 24 October 2013
Available online 2 November 2013

Keywords:
PET imaging
Multiple Sclerosis
Myelin
Cuprizone model
Demyelination
Remyelination

ABSTRACT

Multiple Sclerosis (MS) is a neurodegenerative disease characterized by demyelinated lesions. PET imaging using specific myelin radioligands might solve the lack of a specific imaging tool for diagnosing and monitoring demyelination and remyelination in MS patients. In recent years, a few tracers have been developed for *in vivo* PET imaging of myelin, but they have not been fully evaluated yet. In this study, we compared [^{11}C]CIC and [^{11}C]MeDAS as PET tracers for monitoring demyelination and remyelination in cuprizone-fed mice. The *ex vivo* biodistribution of [^{11}C]CIC showed decreased tracer uptake in mice fed with 0.2% cuprizone diet for 5 weeks, as compared to control mice. However, tracer uptake did not increase again after normal diet was restored for 5 weeks (remyelination). Surprisingly, *in vivo* PET imaging with [^{11}C]CIC in cuprizone-fed mice revealed a significant *reduction* in whole brain tracer uptake after 5 weeks of remyelination. No correlation between *ex vivo* biodistribution and *in vivo* imaging data was found for [^{11}C]CIC ($r^2 = 0.15$, $p = 0.11$). However, a strong correlation was found for [^{11}C]MeDAS ($r^2 = 0.88$, $p < 0.0001$). [^{11}C]MeDAS *ex vivo* biodistribution revealed significant decreased brain uptake in the demyelination group, as compared to controls and increased the tracer uptake after 5 weeks of remyelination. [^{11}C]MeDAS images showed a low background signal and clear uptake in the brain white matter and spinal cord. Taken together, the results of this comparative study between [^{11}C]CIC and [^{11}C]MeDAS clearly show that [^{11}C]MeDAS is the preferred PET tracer to monitor myelin changes in the brain and spinal cord *in vivo*.

Introduction

Multiple Sclerosis (MS) is a disease of the central nervous system with multifocal inflammatory and demyelinated lesions throughout the brain and spinal cord (Inglese and Bester, 2010). The diagnosis of MS is predominantly made based on clinical signs, according to standardized sets of diagnostic criteria (e.g. the McDonald criteria), with Magnetic Resonance Imaging (MRI) as an additional imaging tool (Frullano et al., 2011; WHO, 2008). MRI is based on local changes in water content that can be due to demyelination, but may also reflect inflammation, axonal loss, gliosis and edema (Fillipi and Roca, 2011). A highly specific *in vivo* myelin imaging technique could help to speed up early diagnosis and be used to monitor the efficacy of new drugs aimed at restoring myelin and preventing neurodegeneration. Positron Emission Tomography (PET) is a molecular imaging technique which uses specific ligands labeled with a positron emitter, such as ^{18}F or ^{11}C. If a selective radioligand for a disease-specific target is available, PET can be an excellent tool for diagnosis and for monitoring disease progression with high specificity.

Since 2006, a few ligands have been developed for *in vivo* PET imaging of myelin (Briard et al., 2011; Stankoff et al., 2006; Wang and Wu, 2010; Wang et al., 2009, 2011; Wu et al., 2010). The two most promising radioligands, [^{11}C]CIC and [^{11}C]MeDAS, could be prepared by a reliable labeling procedure, showed high stability and good blood brain barrier penetration and appeared to be able to reveal differences in myelin content in animals. Wu et al. (2006) suggested that the unique structure of myelin, consisting of 80% lipids and a high amount of low-molecular-mass proteins underlies the specific binding of [^{11}C]CIC and [^{11}C]MeDAS to myelin sheaths. Compounds with a stilbene moiety, as is present in [^{11}C]CIC and [^{11}C]MeDAS, were shown to have affinity for β-sheet structures. Myelin basic protein contains β-sheet structures, but only when myelin sheaths are intact. Although these β-sheet structures may contain the binding sites of the PET tracers, the exact binding

Abbreviations: MRI, Magnetic Resonance Imaging; MS, Multiple Sclerosis; PET, Positron Emission Tomography; SUV, Standardized Uptake Value.

* Corresponding author at: Department of Nuclear Medicine and Molecular Imaging, University of Groningen, University Medical Center Groningen, P.O. Box 30.001, Hanzeplein 1, 9713 GZ Groningen, The Netherlands. Fax: +31 50 3611687.
E-mail address: e.f.j.de.vries@umcg.nl (E.F.J. de Vries).

1053-8119/$ – see front matter © 2013 Elsevier Inc. All rights reserved.
http://dx.doi.org/10.1016/j.neuroimage.2013.10.057

mechanism still has not been elucidated yet. Still, a longitudinal [^{11}C]CIC PET study in only a small group of lysolecithin-treated rats managed to reveal focal demyelination (Wang et al., 2009) and [^{11}C]MeDAS PET could detect differences in myelin between wild-type and transgenic hypermyelinated mice (Plp-Akt-DD) (Wu et al., 2010). Recently, imaging of changes in myelin content due to demyelination and remyelination were investigated in the spinal cord, but not in the brain (Wu et al., 2013).

The cuprizone mouse model is a well-established animal model to mimic the demyelination aspect of MS and it is widely used as animal model to investigate the demyelination and remyelination processes (Kipp et al., 2009; Matsushima and Morel, 2001). Feeding mice with 0.2% cuprizone results in demyelination throughout the brain, but in particular in the corpus callosum. When the normal diet is subsequently restored, spontaneous and complete remyelination occurs.

The aim of the present study was to compare [^{11}C]CIC and [^{11}C]MeDAS as PET ligands for monitoring the demyelination and remyelination processes in the cuprizone mouse model.

Material and methods

Animals

Demyelination was induced in 8 week-old C56Bl/6 male mice (Harlan, The Netherlands) by putting them on a diet, consisting of 0.2% cuprizone (bis(cyclohexanone)oxaldihydrazone, Sigma) mixed with powder chow. After 5 weeks, the food was changed again to powder chow without cuprizone to enable spontaneous remyelination. A control group received powder chow without cuprizone during the whole experiment. Every day, powder chow (with or without cuprizone) was freshly prepared and provided to the animals. Food and water were given *ad libitum* and the animals were monitored every day for body weight loss.

The animal experiments were performed according to the Dutch Regulations for Animal Welfare. The protocol was approved by the Institutional Animal Care and Use Committee of the University of Groningen (protocol: DEC 5040l).

Chemistry

The [^{11}C]CIC precursor was synthesized as previously published by Wang and Wu (2010). The [^{11}C]MeDAS precursor was prepared as free base from commercially available 4,4′-diaminostilbene dihydrochloride (Sigma-Aldrich) by treatment with sodium hydroxide 1 M (until pH 10) and extraction using ethyl acetate.

[^{11}C]CIC

[^{11}C]MeOTf was produced as previously described (Elsinga, 2002; Li and Conti, 2010) and transported with a stream of helium gas (30 ml/min) into the reaction vessel containing 0.7–1 mg [^{11}C]CIC desmethyl precursor in 0.5 ml dry acetone (Merck). After the [^{11}C]MeOTf was trapped in the reaction vial, the mixture was heated at 90 °C for 3 min. Acetone was evaporated with a flow of nitrogen gas and the residue was dissolved in 0.5 ml of acetonitrile and diluted with 0.5 ml of water. The product was then purified by HPLC using a reverse-phase C18 platinum column (Alltech) and acetonitrile/25 mM phosphate buffer pH 7.2 (50/50) as the mobile phase (flow 5 ml/min).

The radioactive peak with a retention time of 12 min consisting of purified [^{11}C]CIC was collected from the HPLC and formulated as isotonic solution before injection *in vivo*. For this purpose, the collected HPLC fraction was diluted with 100 ml of distilled water and passed through a SepPak® C18 light cartridge (Waters) that was pre-conditioned with ethanol (8 ml) and water (12 ml). The product was eluted from the cartridge with 1 ml ethanol and diluted with 9 ml 0.9% sodium chloride. The synthesis of [^{11}C]CIC was fully automated using a Zymark robotic system.

During the whole labeling and formulation procedure, exposure of the product to white light was avoided as much as possible to prevent light-induced cis-trans isomerization.

[^{11}C]MeDAS

The radiolabeling procedure for [^{11}C]MeDAS is identical to the procedure described above for [^{11}C]CIC using 4,4′-diaminostilbene (free base) as the precursor. For the HPLC purification, a mixture of acetonitrile and 25 mM phosphate buffer pH 7.2 (35/65) was used as the mobile phase (flow 5 ml/min). The retention time of purified [^{11}C]MeDAS is 8 min.

In contrast to [^{11}C]CIC, [^{11}C]MeDAS does not show rapid light-induced isomerization and therefore the synthesis of this compound can be performed under normal light conditions.

Quality control

Radiochemical purity and specific activity were evaluated by analytical HPLC.

[^{11}C]CIC quality control was performed with an analytical C18 Luna reversed phase HPLC column (Phenomenex) and methanol/water (80/20) as the mobile phase (flow 1 ml/min). The UV signal was measured at a wavelength of 254 nm. The retention time of [^{11}C]CIC is 12 min.

[^{11}C]MeDAS quality control was performed using an analytical C18 X-Terra reversed phase HPLC column (Waters) and acetonitrile/30 mM ammonium acetate pH 10.0 (15/85) as mobile phase (flow 1.5 ml/min). UV measured at a wavelength of 254 nm. The retention time of [^{11}C]MeDAS is 14 min.

PET imaging and ex vivo biodistribution

Mice were divided into 4 groups for small animal PET imaging (each n = 6) and ex-vivo biodistribution (each n = 5) studies of both myelin PET tracers: group 1: controls — animals fed with powder food without cuprizone, age matched with the demyelination group at the moment of imaging and biodistribution (13 weeks old); group 2: demyelination — animals fed with 0.2% cuprizone for 5 weeks; group 3: early remyelination — animals fed with 0.2% cuprizone for 5 weeks followed by a normal diet for another 2 weeks; group 4: late remyelination — animals fed with 0.2% cuprizone for 5 weeks followed by a normal diet for another 5 weeks.

For small animal PET imaging, mice were anesthetized with 2% isoflurane in medical air and injected with 10–30 MBq of either [^{11}C]CIC or [^{11}C]MeDAS in the penile vein. After tracer injection, the mice were immediately positioned on their belly in the microPET camera (Focus 220, Siemens Medical Solutions USA, Inc.) with the head in the field of view.

Five minutes after tracer injection, acquisition of a 50-min dynamic PET scan was started (time 0 represents the time of tracer injection). After the emission scan was completed, a transmission scan of 515 s with a ^{57}Co point source was performed for attenuation and scatter correction.

After the transmission scan, animals were terminated by extirpation of the heart and the brain was excised for *ex-vivo* biodistribution (n = 5 for each tracer) and histological analysis (n = 1 for each tracer).

Brain biodistribution analysis was performed 60–65 min after tracer injection. Each brain was dissected in the following regions: cerebellum, pons, medulla, corpus callosum, hippocampus, striatum and the rest of the brain (for calculating whole brain tissue uptake). Tissues were weighed and radioactivity was measured in a gamma counter (LKB Wallac, Turku, Finland). Tracer uptake in each region was corrected for the injected tracer dose and body weight and expressed as Standardized Uptake Value (SUV).

PET image reconstruction and analysis

The list-mode data of the emission scan was separated into 25 frames (8 × 30, 6 × 60, 4 × 120, 4 × 180, 2 × 300 and 1 × 600). Emission sinograms were iteratively reconstructed (OSEM2d, 4 iterations) after being normalized, corrected for attenuation and decay of radioactivity. PET images were analyzed by INVEON research workstation software (Siemens). Regions of interest were drawn for the whole brain. The brain radioactivity concentration was calculated from the regions of interest to generate the brain time-activity curves. Time activity curves were corrected for injected dose and animal body weight and expressed as SUV. The last 10 min frame (45–55 min post injection) was used to show the SUV differences between the groups.

Myelin histochemistry

For histological analysis, the animals (1 mouse per tracer for each experimental condition: thus in total 2 animals per condition) were perfused with 4% paraformaldehyde before termination. Brains were equilibrated in 20% sucrose and cryosectioned in the coronal plane at 20 μm thickness. Changes in the level of myelination of the corpus callosum were detected by Luxol Fast Blue histochemistry. A Luxol Fast Blue solution was prepared by dissolving 0.5 g of Solvent Blue 38 (Sigma) in 500 ml of a solution of 10% acetic acid in 96% ethanol. Sections were dehydrated in an ascending ethanol series (50%, 70%, 80% and 96%) and incubated in the Luxol Fast Blue solution at 58 °C for 14–16 h. After incubation, sections were washed with 96% ethanol and distilled water. Differentiation was performed in a 0.125% lithium carbonate solution, after which the sections were rinsed with 70% ethanol and distilled water, counterstained with cresyl violet and coverslipped with DePeX (Merck). Slides were analyzed with a Zeiss fluorescent microscope.

Statistical analysis

Results are presented as mean ± standard deviation. Differences between groups were analyzed by 2 way ANOVA (GraphPad Prism), using a Bonferroni post hoc test. Differences between groups were considered to be significant if $p < 0.05$.

Results

Radiolabeling

[^{11}C]CIC was labeled using [^{11}C]methyl triflate instead of [^{11}C]methyl iodide, as was previously published by Wang and Wu (2010). The use of [^{11}C]MeOTf allowed milder reaction conditions, increased the radiochemical yield, decreased the amount of precursor required and reduced the total synthesis time of the procedure. The advantages of this new labeling method are summarized in Table 1.

Table 1
Advantages of using [^{11}C]methyl triflate, instead of [^{11}C]methyl iodide, for radiolabeling of [^{11}C]CIC.

	[^{11}C]Methyl iodide (Wang and Wu, 2010)	[^{11}C]Methyl triflate
Precursor	2 mg	0.7–1.0 mg
Base	K_2CO_3	Not required
Reaction time	10 min	3 min
Reaction temperature	140 °C	90 °C
Filtration before HPLC	Yes	No
Total synthesis time (from trapping)	40-50 min	20-30 min
Radiochemical purity	>95%	>95%
Yield (decay corrected from radioactivity trapped)	20%–32%	30%–37%

We observed that light induced substantial cis-trans isomerization of the central double bond. However, when the radiosynthesis of [^{11}C]CIC was performed in the dark, high radiochemical yield (30–37%), high radiochemical purity (>95%) and high specific activity (90 ± 55 GBq/μmol) were obtained. The purified trans-isomer of the product was stored in the dark to avoid isomerization before injection.

[^{11}C]MeDAS radiolabeling was performed as described by Wu et al. (2010) and similar results were obtained. The radiochemical yield was 45–55%, the radiochemical purity >95% and the specific activity 133 ± 56 GBq/μmol.

Ex-vivo biodistribution

The brain distribution was determined for each tracer in four experimental groups, allowing the evaluation of myelin content in normal conditions (control), loss of myelin (demyelination) and recovery of myelin (early and late remyelination).

Fig. 1 shows the [^{11}C]CIC *ex vivo* brain distribution for the different groups 60–65 min after tracer injection. Only in the corpus callosum, a significant decrease (−44%, $p < 0.001$) in tracer uptake was observed after 5 weeks of cuprizone diet (demyelination), but tracer uptake did not rise back to normal levels after normal diet was restored for 2 weeks (early remyelination) or for 5 weeks (late remyelination).

[^{11}C]MeDAS showed a significant decrease in brain uptake after feeding the mice with a 0.2% cuprizone diet for 5 weeks (Fig. 2). The decrease in tracer uptake was largest (−68%, $p < 0.001$) in the corpus callosum where the effect of the cuprizone diet on myelin levels is most prominent (Matsushima and Morel, 2001). The uptake of [^{11}C]MeDAS was restored to normal levels after 5 weeks of normal diet (without cuprizone), reflecting the spontaneous remyelination in this model. No significant increase in tracer uptake was seen after only 2 weeks of normal diet, suggesting that remyelination is still incomplete at this stage.

PET imaging

In order to assess the ability of [^{11}C]CIC or [^{11}C]MeDAS to visualize the demyelination and remyelination processes, cuprizone-fed mice were imaged with both tracers using a dedicated PET camera for small animals. The myelin PET tracers showed clear differences in *in vivo* distribution. [^{11}C]CIC showed significant background uptake in extra-cerebral structures, resulting in a low brain-to-background uptake ratio (Fig. 3A). For [^{11}C]MeDAS (Fig. 3B), on the other hand, the background uptake in extra-cerebral tissues was much lower. Consequently, not only myelin in the brain, but also in the spinal cord, a myelin rich part of the central nervous system, was clearly visible on the PET images.

The tracer kinetics of both tracers are also markedly different. [^{11}C]CIC rapidly accumulates in the brain and reaches a plateau within 10 min after tracer injection (Fig. 4). The tracer accumulation in the brain, expressed as SUV, was significantly different only for the late remyelination group, which showed lower uptake than the control ($p < 0.01$), demyelination ($p < 0.01$) and early remyelination ($p < 0.001$) groups (SUV 45–55 min: 0.74 ± 0.04, 0.99 ± 0.15, 1.01 ± 0.11 and 1.16 ± 0.06, respectively). The area under the time–activity curves confirmed the SUV results, as no significant differences were found between the control (48.7 ± 7.7) and demyelination (51.7 ± 7.1) groups, and the early remyelination group (58.9 ± 1.9). Remarkably, the late remyelination group did show a significantly reduced area under the curve (34.6 ± 1.6). Thus, the [^{11}C]CIC uptake did not reflect the expected myelin content in the brain and did not correlate well ($r^2 = 0.15$, $p = 0.11$) with the *ex vivo* biodistribution results (Fig. 6A). In contrast to [^{11}C]CIC, [^{11}C]MeDAS shows rapid washout from the brain (Fig. 5), resulting in a lower brain uptake with SUV values (45–55 min) of 0.30 ± 0.04, 0.26 ± 0.02, 0.28 ± 0.02 and

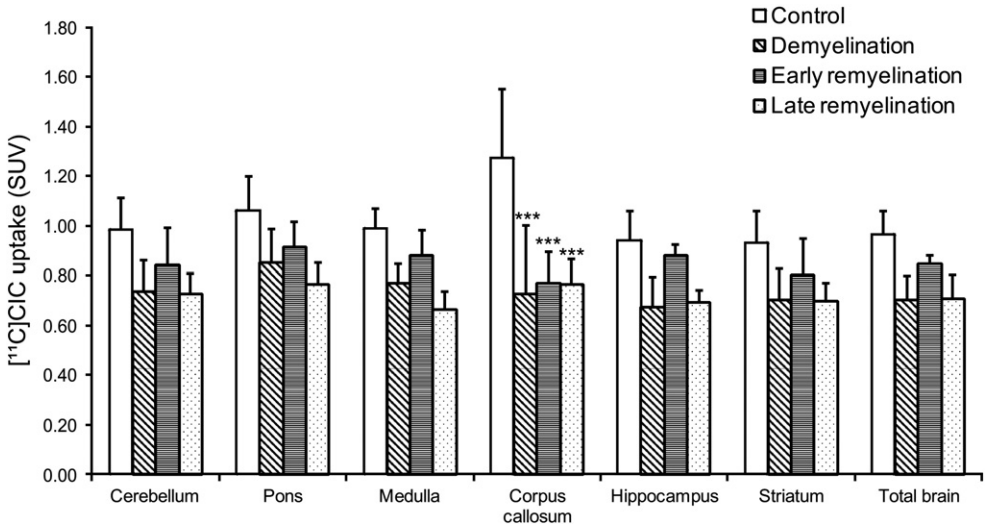

Fig. 1. [^{11}C]ClC *ex vivo* biodistribution (n = 5) in different brain regions of the control, demyelination (5 weeks on cuprizone 0.2% diet) and early and late remyelination groups (2 weeks and 5 weeks back to normal diet, respectively). Significant differences compared to controls are illustrated by *** ($p < 0.001$). No significant differences were observed between the demyelination and remyelination groups.

0.35 ± 0.05 for the control, demyelination, early and late remyelination group, respectively. The SUV of [^{11}C]MeDAS (45–55 min) in the late remyelination group was significantly higher than in the demyelination group ($p < 0.05$), reflecting the increase in myelin density during remyelination. The area under the time–activity curves of [^{11}C]MeDAS are in agreement with the expected myelin density in the brain, with the highest values for the control group (28.9 ± 2.6) and late remyelination group (31.9 ± 4.3) and significantly lower values (as compared to the late remyelination group), for the demyelination group (25.9 ± 1.9, $p < 0.05$) and the early remyelination group (26.6 ± 2.8, $p < 0.05$). The whole brain uptake of [^{11}C]MeDAS as determined by PET correlated strongly with whole brain *ex vivo* biodistribution data ($r^2 = 0.88$, $p < 0.0001$; Fig. 6B).

Histochemistry

Luxol Fast Blue staining for myelin was used to validate the PET imaging data of the demyelination and remyelination progression in the cuprizone mouse model. Fig. 7 shows coronal sections of the corpus callosum at the level of the hippocampus for the different groups, illustrating the demyelination and remyelination in the cuprizone mouse model over time. The corpus callosum in control animals shows compact myelin (dark blue), whereas in the demyelination group areas of complete demyelination can be seen. Histochemistry of sections from the remyelination groups suggests only minor myelin recovery after 2 weeks, but more advanced remyelination of the corpus callosum after 5 weeks.

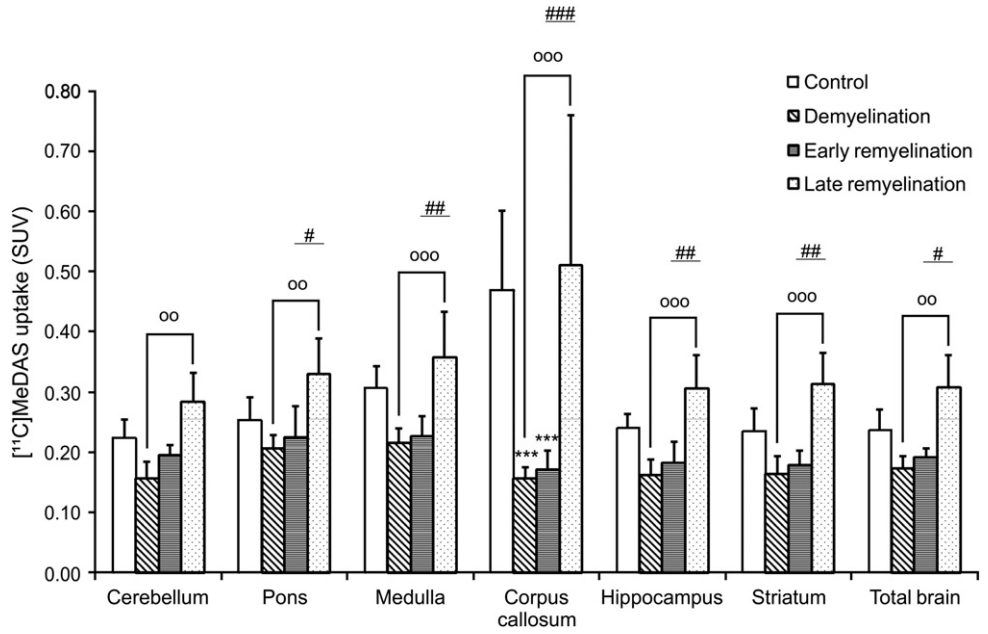

Fig. 2. [^{11}C]MeDAS *ex vivo* biodistribution (n = 5) in different brain regions of the control, demyelination (5 weeks on cuprizone 0.2% diet) and early and late remyelination groups (2 weeks and 5 weeks back to normal diet, respectively); Significant differences are illustrated by *** ($p < 0.001$) for the comparison of the demyelination and remyelination groups with controls, by °° ($p < 0.01$) and °°° ($p < 0.001$) for the comparison between demyelination and late remyelination and by # ($p < 0.05$), ## ($p < 0.01$) and ### ($p < 0.001$) for the comparison between early and late remyelination.

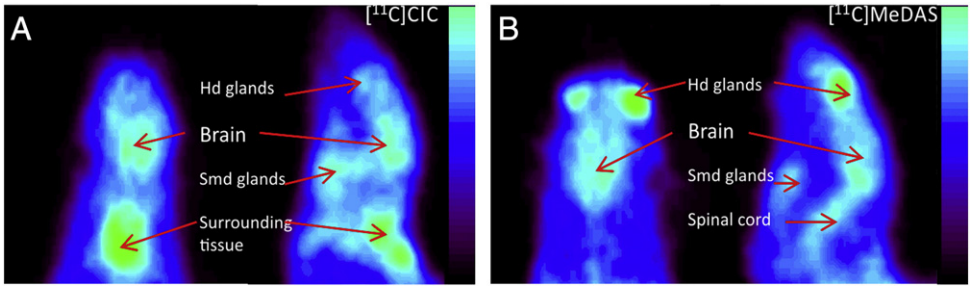

Fig. 3. Illustrative coronal (left) and sagittal (right) PET images (summed 35–55 min images) of control mice using [^{11}C]CIC (A) and [^{11}]MeDAS (B). Structures are indicated by arrows: Hd glands = harderian glands; brain; Smb glands = submandibular glands; spinal cord and surrounding tissue.

Discussion

Positron Emission Tomography could provide a valuable tool for imaging ongoing demyelination processes in the central nervous system of MS patients. Quantification of myelin content, using myelin-specific PET tracers, could facilitate the MS diagnosis and allow the monitoring of disease progression and treatment efficacy. In this study, we aimed to compare [^{11}C]CIC and [^{11}C]MeDAS as PET tracers for quantification of myelin content during the demyelination and remyelination processes in cuprizone-fed mice.

Compounds with a stilbene structure, such as BMB, BDB, CIC and MeDAS, have been shown to bind to amyloid-like proteins with aggregated β-sheet structures. This β-sheet structure is also found in the myelin basic protein, when myelin sheaths are intact. The binding sites of these compounds to myelin have still to be determined. However, the theory is that once myelin degenerates (demyelination), the β-sheet structure of myelin basic protein is lost and consequently tracer binding decreases (Wu et al., 2006).

[^{11}C]CIC was described (Wang et al., 2009) as an improved tracer as compared to [^{11}C]BMB – the first ligand used as myelin PET tracer for animal imaging (Stankoff et al., 2006) – due to its easy labeling with [^{11}C], high stability and easy dissolution in organic solvents. We optimized the procedure for labeling [^{11}C]CIC, using methyl triflate as the alkylating agent. As a result, the synthesis was faster with a better yield, using less amounts of precursor and a lower reaction temperature (Table 1) in comparison to the procedure with [^{11}C]methyl iodide as methylating agent that was described by Wang et al. (2009). We observed that [^{11}C]CIC was not stable when exposed to light, as light induced reversible cis-trans isomerization of the labeled product. This side-reaction could be prevented by performing the synthesis in the dark. After the synthesis, exposure of the product to light was kept to a minimum. In this manner, the trans isomer of [^{11}C]CIC was obtained with a radiochemical purity higher than 95%.

Previous studies on *in vivo* imaging of lysolecithin-induced demyelination in rats with [^{11}C]CIC showed promising results (Wang et al., 2009). Therefore, we selected this tracer for further evaluation and for comparison with another promising tracer, [^{11}C]MeDAS. We evaluated both tracers in the demyelination/remyelination cuprizone mouse model.

[^{11}C]CIC *ex vivo* biodistribution showed a significant decrease in brain uptake after 5 weeks on the cuprizone diet, reflecting the well-documented demyelination induced by the oligodendrocyte-selective toxin cuprizone (Matsushima and Morel, 2001). However, restoring the diet to normal powder chow, known to induce spontaneous remyelination, did not result in the expected increase in tracer uptake to control levels. The fact that myelin layers are, in general, thinner and less compact immediately after remyelination (Ohama et al., 1990; Patrikios et al., 2006; Shrager, 1988), may explain the absence of a clear increase in tracer uptake after 2 weeks on normal diet, but this phenomenon cannot explain why no increase in uptake was observed in the late remyelination group. In fact, histochemistry proved that the restored myelin layers in this late remyelination group were comparable to the control group. Small animal PET imaging showed a good brain uptake, but slow washout tracer kinetics. This characteristic is a disadvantage for ^{11}C-labeled PET tracers, since slow washout results in longer acquisition times, which is not compatible with short half-life isotopes such as ^{11}C (20 min) (Koeppe, 2007). Another problem with [^{11}C]CIC was that PET imaging data (SUV or area under the curve) did not reflect myelin content as determined by histochemistry at all, nor did imaging data correlate with *ex vivo* biodistribution data

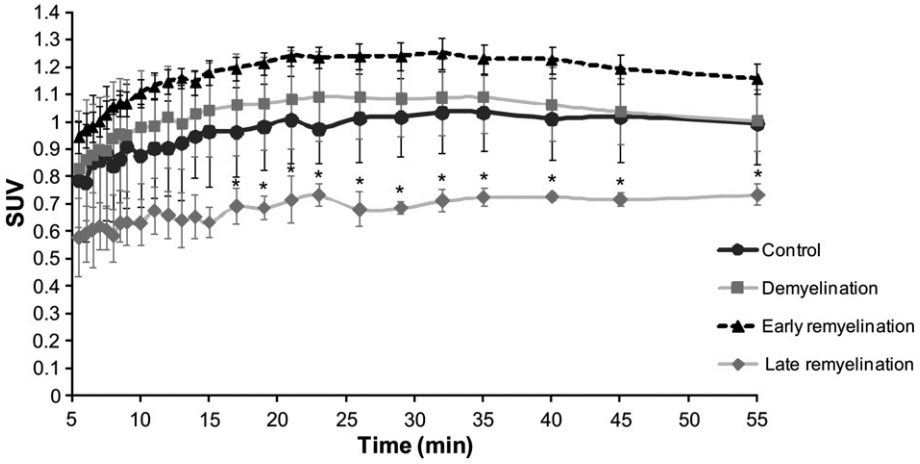

Fig. 4. [^{11}C]CIC time activity curve of different groups (n = 6); control, demyelination after 5 weeks on cuprizone 0.2% diet, early remyelination after 2 weeks on normal diet and late remyelination after 5 weeks on normal diet. The PET camera was started 5 min after tracer injection. Significant differences between the late remyelination group and the other groups are illustrated by * ($p < 0.05$).

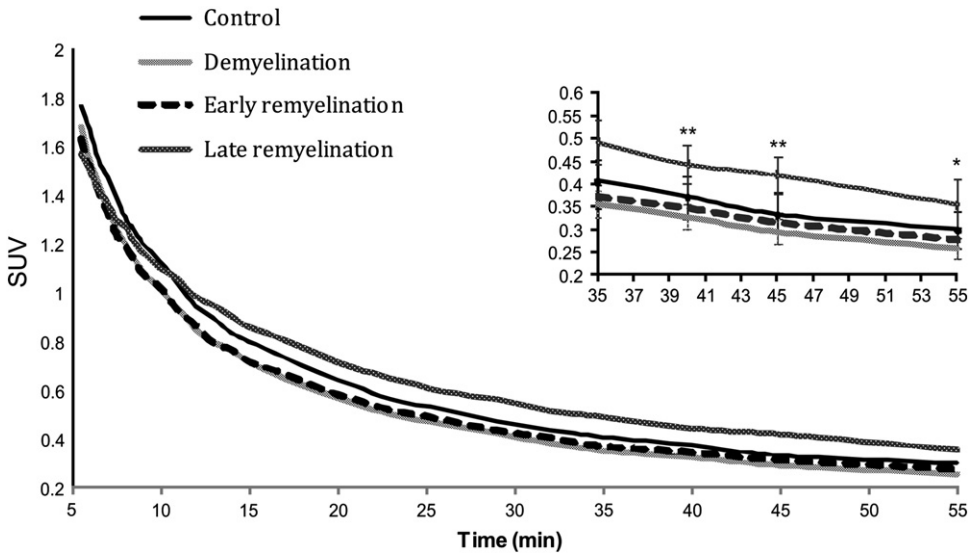

Fig. 5. [^{11}C]MeDAS time activity curve of different groups (n = 6); control, demyelination 5 weeks on cuprizone 0.2% diet, early remyelination after 2 weeks on normal diet and late remyelination after 5 weeks on normal diet. The insert shows the last 20 min of the scan in more detail. The PET camera was started 5 min after tracer injection. Significant differences between the late remyelination group and the demyelination group are illustrated by ** ($p < 0.01$) and * ($p < 0.05$).

($r^2 = 0.15$, $p = 0.11$). Probably, the high radioactivity levels in surrounding tissues may have caused spill-over effects, which could explain the discrepancy between the *in vivo* PET imaging results and the *ex vivo* biodistribution data (Herrero et al., 1989; Muzic et al., 1998). Another drawback for using [^{11}C]CIC for PET imaging is the fact that the spinal cord, a central nervous system structure rich in myelin, could not be visualized in *in vivo* images. It should be mentioned that part of the poor [^{11}C]CIC PET results in our study might be related to the low amount of myelin content in mouse brain (Zhang and Sejnowski, 2000) in comparison to rat brain used in the lysolecithin studies of Wang et al. (Wang et al., 2009).

The original paper describing the use of [^{11}C]MeDAS for myelin PET imaging (Wu et al., 2010) showed brain images that clearly reflected the differences in myelin content between wild type mice and hypermyelinated transgenic Plp-Akt-DD mice. The same group described in a recent paper (Wu et al., 2013) that [^{11}C]MeDAS is also able to show changes in myelin in the spinal cord, but the demyelination and remyelination processes in the brain in an animal model like the lysolecithin or our cuprizone model have not been investigated with this tracer yet.

We performed the [^{11}C]MeDAS radiosynthesis by the easy and reproducible radiolabeling of the commercially available compound 4,4-diaminostilbene with [^{11}C]methyl triflate, according to the already published method by Wu et al. (2010). In this study, we obtained comparable results as described by Wu.

Ex vivo biodistribution of [^{11}C]MeDAS (Fig. 2) showed a decrease in tracer uptake in the corpus callosum of mice that were fed with a 0.2% cuprizone diet for 5 weeks. The decrease in uptake in other brain regions was also present but was not statically significant. In contrast to [^{11}C]CIC, *ex vivo* biodistribution of [^{11}C]MeDAS revealed the spontaneous remyelination in the corpus callosum and in other brain regions such as the cerebellum, pons, medulla, hippocampus and striatum, which are regions known to be affected by the cuprizone diet (Steelman et al., 2012). The fact that the differences in tracer uptake in other brain regions were significant between the demyelination group and the late remyelination, but not between the demyelination group and the control group may be explained by differences in age between controls and the late remyelination group. In mice, the myelin density keeps increasing with age until the animals are around 9 months old (Calderini et al., 1983). The control group was age matched with the 5 week demyelination group (13 weeks old). However, the late remyelination group was 5 weeks older, which may have caused a slightly higher myelin density due to the natural myelination process in addition to the spontaneous remyelination after removal of the cuprizone from the diet.

Small animal PET imaging using [^{11}C]MeDAS revealed fast kinetics, allowing image acquisition soon after injection (favorable for ^{11}C-labeled tracers) and a high target-to-background ratio. On the other hand the fast washout of [^{11}C]MeDAS resulted in relatively low SUV values at the end of the scan, complicating the detection of

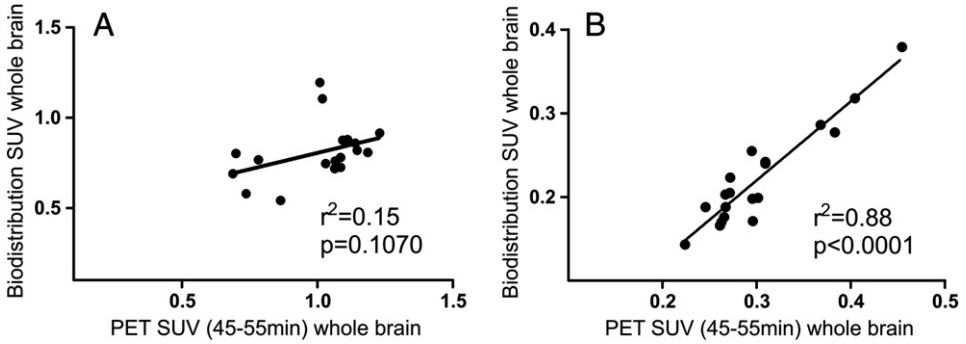

Fig. 6. Correlation between whole brain tracer uptake (SUV) as determined by PET (45–55 min after tracer injection) and by *ex vivo* biodistribution (60–65 min). The animals of all experimental groups (4 groups), for which both PET and *ex vivo* biodistribution data were available (5 animals per group), were included in the correlation. (A) [^{11}C]CIC, (B) [^{11}C]MeDAS.

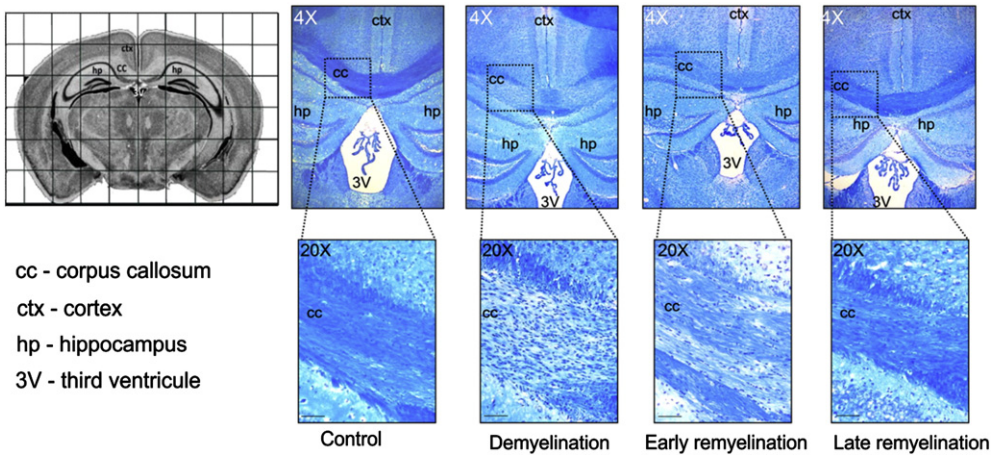

Fig. 7. Myelin histochemistry, using Luxol Fast Blue staining, in the corpus callosum (cc) at the hippocampus (hp)/third ventricle (3V) level (region illustrated by the top left image — adapted from www.mbl.org; grid = 1 mm). The lower row depicts magnifications of areas indicated in the upper row (scale bar = 100μm). From left to right: control corpus callosum, corpus callosum after 5 weeks on 0.2% cuprizone diet (demyelination), corpus callosum 2 weeks after restoring normal diet (early remyelination) and corpus callosum 5 weeks after normal diet was restored (late remyelination).

significant differences between the groups. Significant differences were observed only between the demyelination group and the late remyelination group (last 30 min of the scan). The area under the time-activity curve however did show significant differences between the demyelination and the late remyelination group ($p < 0.05$) and also between the early and the late remyelination groups ($p < 0.05$). PET imaging data strongly correlated with the *ex vivo* biodistribution data ($r^2 = 0.88$, $p < 0.0001$) and were in close agreement with histochemical findings.

In this study, PET data were expressed as SUV, which is sensitive to several factors, such as tracer delivery and metabolism. To correct for these variables, pharmacokinetic modeling could be applied. However, repetitive arterial blood sampling to obtain the input function is problematic in mice, due to the small total blood volume. In a parallel study in rats (data will be published elsewhere), we observed that the distribution volume (Logan analysis) showed an excellent correlation with the SUV for [^{11}C]MeDAS, but not for [^{11}C]CIC, suggesting that correction for tracer input and metabolism may improve the performance of [^{11}C]CIC.

Another limitation of PET imaging in mice is that the resolution of the PET camera does not allow discrimination between gray and white matter in the small mouse brain. Consequently, PET data comprise both gray and white matter. Since white matter is richer in myelin than gray matter, PET will give an underestimation of the myelin changes in white matter. In fact, we observed that the differences between groups were larger for *ex vivo* biodistribution than for PET. This issue becomes less important when PET imaging of myelin is applied in larger animals or humans.

Conclusion

Our head-to-head comparison of [^{11}C]CIC and [^{11}C]MeDAS as potential PET tracers for imaging of myelin changes in the brain, revealed clear differences in imaging properties between both tracers. [^{11}C]MeDAS showed much faster tracer clearance from non-target tissues. Although both [^{11}C]CIC and [^{11}C]MeDAS were able to detect ongoing demyelination, only [^{11}C]MeDAS was able to show remyelination. Moreover, only [^{11}C]MeDAS PET imaging data correlated well with *ex vivo* biodistribution data and histochemistry. These properties, together with the easier labeling procedure, make [^{11}C]MeDAS the preferred myelin PET tracer for *in vivo* PET imaging of myelin density.

Acknowledgments

We would like to thank the Dutch MS Research Foundation (project 10–0700 MS) for financial support, Inês Farinha Antunes, Bram Maas and Chantal Kwizera for the assistance during radiolabeling optimization and Ietje Mantingh-Otter for helping with histochemistry techniques.

References

Briard, E., Orain, D., Beerli, C., Billich, A., Streiff, M., Bigaud, M., Auberson, Y.P., 2011. BZM055, an iodinated radiotracer candidate for PET and SPECT imaging of myelin and FTY720 brain distribution. ChemMedChem 6, 667–677.
Calderini, G., Bonetti, A.C., Battistella, A., Crews, F.T., Toffano, G., 1983. Biochemical changes of rat brain membranes with age. Neurochem. Res. 8 (4), 483–492.
Elsinga, P.H., 2002. Radiopharmaceutical chemistry for positron emission tomography. Methods 27, 208–217.
Fillip, M., Rocca, M.S., 2011. MR imaging of multiple sclerosis. Radiology 259 (3), 659–681.
Frullano, L., Wang, C., Miller, R.H., Wang, Y., 2011. A myelin-specific contrast agent for magnetic resonance imaging of myelination. J. Am. Chem. Soc. 133, 1611–1613.
Herrero, P., Markham, J., Bergmann, S.R., 1989. Quantitation of myocardial blood flow with 215O and positron emission tomography: assessment and error analysis of a mathematical approach. J. Comput. Assist. Tomogr. 13 (5), 862–873.
Inglese, M., Bester, M., 2010. Diffusion imaging in multiple sclerosis: research and clinical implications. NMR Biomed. 23, 865–872.
Kipp, M., Clarner, T., Dang, J., Copray, S., Beyer, C., 2009. The cuprizone animal model: new insights into an old story. Acta Neuropathol. 118, 723–736.
Koeppe, R.A., 2007. In: Maguire, R.P., Leenders, K.L. (Eds.), PET Pharmacokinetic Course Manual (Chapter 11, Kobe, Japan).
Li, Z., Conti, P.S., 2010. Radiopharmaceutical chemistry for positron emission tomography. Adv. Drug Deliv. Rev. 62, 1031–1051.
Matsushima, G.K., Morel, P., 2001. The neurotoxicant, cuprizone, as a model to study demyelination and remyelination in the central nervous system. Brain Pathol. 11, 107–116.
Muzic Jr., R.F., Chen, C.-H., Nelson, A.D., 1998. A method to correct for scatter, spillover, and partial volume effects in region of interest analysis in PET. IEEE Trans. Med. Imaging 17, 202–213.
Ohama, E., Horikawa, Y., Shimizu, T., Morita, T., Nemoto, K., Tanaka, H., Ikuta, F., 1990. Demyelination and remyelination in spinal cord lesions of human lymphotropic virus type I-associated myelopathy. Acta Neuropathol. 81, 78–83.
Patrikios, P., Stadelmann, C., Kutzelnigg, A., Rauschka, H., Schmidbauer, M., Laursen, H., Sorensen, P.S., Brück, W., Lucchinetti, C., Lassmann, H., 2006. Remyelination is extensive in a subset of multiple sclerosis patients. Brain 129, 3165–3172.
Shrager, P., 1988. Ionic channels and signal conduction in single remeylination frog nerve fibers. J. Physiol. 404, 695–712.
Stankoff, B., Wang, Y., Bottlaender, M., Aigrot, M.S., Dolle, F., Wu, C., Feinstein, D., Huang, G.F., Semah, F., Mathis, C.A., Klunk, W., Gould, R.M., Lubetzki, C., Zalc, B., 2006. Imaging of CNS myelin by positron-emission tomography. PNAS 103 (24), 9304–9309.
Steelman, A.J., Thompson, J.P., Li, J., 2012. Demyelination and remyelination in anatomically distinct regions of the corpus callosum following cuprizone intoxication. Neurosci. Res. 72 (1), 32–42.
Wang, Y., Wu, C.H., 2010. *In vivo* imaging of myelination. Patent number US2010/0221180 A1.

Wang, Y., Wu, C., Caprariello, A.V., Somoza, E., Zhu, W., Wang, C., Miller, R.H., 2009. *In vivo* quantification of myelin changes in the vertebrate nervous system. J. Neurosci. 29 (46), 14663–14669.

Wang, C., Wu, C., Zhu, J., Miller, R.H., Wang, Y., 2011. Design, synthesis, and evaluation of coumarin-based molecular probes for imaging of myelination. J. Med. Chem. 54 (7), 2331–2340.

WHO — World Health Organization, 2008. Atlas Multiple Sclerosis Resources in the World. 978 92 4 156375 8.

Wu, C., Tian, D., Feng, Y., Polak, P., Wei, J., Sharp, A., Stankoff, B., Lubetzki, C., Zalc, B., Mufson, E.J., Gould, R.M., Feinstein, D.L., Wang, Y., 2006. A novel fluorescent probe that is brain permeable and selectively binds to myelin. J. Histochem. Cytochem. 54, 997–1004.

Wu, C., Wang, C., Popescu, D.C., Zhu, W., Somoza, E.A., Zhu, J., Condie, A.G., Flask, C.A., Miller, R.H., Macklin, W., Wang, Y., 2010. A novel PET marker for *in vivo* quantification of myelination. Bioorg. Med. Chem. 18, 8592–8599.

Wu, C., Zhu, J., Baeslack, J., Zaremba, A., Hecker, J., Kraso, J., Matthews, P.M., Miller, R.H., Wang, Y., 2013. Longitudinal PET imaging for monitoring myelin repair in the spinal cord. Ann. Neurol. http://dx.doi.org/10.1002/ana.23965 (Epub ahead of print).

Zhang, K., Sejnowski, T.J., 2000. A universal scaling law between gray matter and white matter of cerebral cortex. PNAS 97, 5621–5626.